Electrochimica Acta 212 (2016) 147–154

Contents lists available at ScienceDirect

Electrochimica Acta

journal homepage: www.elsevier.com/locate/electacta

A novel sensitive electrochemical sensor for lead ion based on three-dimensional graphene/sodium dodecyl benzene sulfonate hemimicelle nanocomposites

Na Qiu[a,b], Yan Liu[a,*], Rong Guo[a,*]

[a] School of Chemistry and Chemical Engineering, Yangzhou University, Yangzhou, 225002, Jiangsu, PR China
[b] College of Chemistry Chemical Engineering and Material Science, Zaozhuang University, Zaozhuang 277160, Shandong, PR China

ARTICLE INFO

Article history:
Received 13 April 2016
Received in revised form 23 June 2016
Accepted 26 June 2016
Available online 27 June 2016

Keywords:
3D graphene
hemimicelle
nanocomposite
lead ion
voltammetry

ABSTRACT

For the first time, a novel lead ion electrochemical sensor based on three-dimensional grapheme foam/sodium dodecyl benzene sulfonate hemimicelle (3D GF/SDBS HM) nanocomposite has been developed. This nanocomposite was characterized by scanning electron microscopy (SEM), X-ray diffraction (XRD), Fourier transform-infrared (FTIR) spectroscopy and contact angle measurements, which demonstrated that SDBS hemimicelles were attached on the surface of the 3D graphene foam. Electrochemical properties of the nanocomposite modified electrode were characterized by cyclic voltammetry and electrochemical impedance spectroscopy. This electrochemical sensing interface exhibited excellent stripping performance for the analysis of Pb^{2+} with the detection limit of 0.0145 nM, combining the advantageous of 3D graphene foam (well-defined macroporous structure, high electrical conductivity and specific area) together with the unique accumulating and depositing features of hemimicelle. The sensor was further applied to the determination of lead ion in real water samples with satisfactory results.

1. Introduction

The sensitive, rapid, low-cost, and simple detection of heavy metal ions has been attracting increasing attention in environmental, industrial and biomedical applications, since they have a significantly negative effect on living organism [1,2]. Among many analytical procedures developed to detect trace heavy metal ions, the electrochemical stripping analysis, have been widely recognized as a powerful tool due to its low cost, short analysis time, easy operation, high sensitivity, and good portability [3]. Traditionally, mercury electrodes have been used in the electrochemical stripping analysis due to the high sensitivity. Because of the high toxicity of mercury, the use of mercury electrode is not favorable.

To obtain the desired limit of detection in the stripping analysis, it is important to find a proper and efficient nanomaterial to modify the electrode surface [4,5]. An efficient modified nanomaterial should have the ability to accumulate heavy metal ions, and provide the conduction pathways for electrons effectively on electrode surface. Graphene, owing to its excellent electrical properties and high surface area, is extremely attractive in sensors [6]. Unfortunately, graphene easily suffers from aggregation and stacking after removal of dispersed solutions and drying due to the van der Waals interactions, which restrict its electrochemical sensing application to some extent. Very recently studies demonstrate that chemical vapor deposition-grown three-dimensional graphene foams (3D GF) are seamlessly continuous and a highly conductive graphene network without defects and intersect junctions [7–9]. To enhance the unique properties of graphene materials and exploit their electrochemical sensing, 3D GF have recently attracted increasing attention due to their unique structure and properties [10–12]. However, 3D GF materials have a low affinity for heavy metal ions due to the highly hydrophobic surfaces, which hinders its application in heavy metal ion detection [13].

So far, the adsorption behavior of surfactants on hydrophobic graphene surfaces has been deeply investigated [14–16]. Generally, the surfactants adsorbed on a hydrophobic surface tend to aggregate into half-cylindrical hemimicelles above the critical surface aggregation concentration (csac) on hydrophobic graphene surfaces in aqueous solution from both the experimental observations and computer simulations [14–16]. In these

* Corresponding authors. Tel.: +86 514 87971802; fax: +86 514 87311374.
E-mail addresses: yanliu@yzu.edu.cn (Y. Liu), guorong@yzu.edu.cn, guorong@yzu.edu.cn (R. Guo).

http://dx.doi.org/10.1016/j.electacta.2016.06.136
0013-4686/

aggregates, the headgroup of the adsorbed surfactant molecules are exposed to the aqueous phase in the high-density adsorption regime. Hemimicelles have aroused considerable interest in the field of sensor and separation science [17–20]. Although hemimicelle adsorbed on hydrophilic surfaces has been widely used to concentrate and detect small organic molecules in aqueous solution [21–23], hemimicelle adsorbed on hydrophobic surfaces has hardly been used in sensors. Some earlier studies have indicated that anionic surfactants such as sodium dodecyl benzenesulfonate and sodium dodecyl sulfate have a high affinity toward heavy metal ions [24–26]. Therefore, if we combine the advantages of anionic surfactant hemimicelles (the high affinity towards heavy metal ions) and 3D GF (well-defined macroporous structure, high electrical conductivity and specific area) to fabricate nanocomposites, a new opportunity for excellent electrochemical sensing performance in heavy metal ions detection is provided. The aim of this work is to develop a simple and ultrasensitive lead ion electrochemical sensor based on anionic surfactant hemimicelle/3D graphene nanocomposite modified glass carbon electrode. This will not only offer simple and convenient procedures to modify the hydrophobic 3D GF, and but also will extend the scope of application of hemimicelle-based sensor.

In this work, we demonstrated that the electrode modified with 3D GF/SDBS HM nanocomposite was used for accumulation and sensitive detection of trace lead ions. As shown in Scheme 1, 3D graphene foam aligned on the GC electrode served as the hard and robust supports for the half-cylindrical hemimicelles formed by sodium dodecyl benzenesulfonate (SDBS), and the half-cylindrical hemimicelles could further act as adsorbents to rapidly concentrate and deposite lead ions from aqueous solution to electrode surface. Furthermore, the well-defined macroporous structure and high electrical conductivity of 3D GF allows the quantitative determination of Pb^{2+} by means of stripping voltammetry current effectively.

2. Experimental section

2.1. Reagents and chemicals

Sodium dodecyl benzene sulfonate (SDBS) was obtained from Sigma-Aldrich. The standard stock solution of Pb^{2+} (100 mg L^{-1}) was obtained from Aladdin Reagent Co. All other reagents and chemicals were reagent grade and used for the following experiment directly. Deionized water (18.2 MΩ) was used throughout. The nickel foam was obtained from Jiashide Technology (Suzhou), PPI: 110; thickness: 1.5 mm; density: 400 g/m^2.

2.2. Preparation of 3D graphene foam

As previously described [12], 3D GF was synthesized by chemical vapor deposition method with nickel foam as the growth substrate and ethanol as the carbon source under atmosphere pressure. The nickel foam placed into a quartz tube was heated to 1000 °C at a 30 °C/min heating rate and maintained for 30 min under atmospheric pressure with a gas flow of H_2/Ar (H_2/Ar = 30:300 sccm) to clean the surface of nickel foam. The ethanol was introduced into the CVD chamber by a bubbling system with 50 sccm Ar gas. After 15 min of growth, the sample was rapidly cooled to the room temperature at a cooling rate of 100 °C/min under H_2/Ar flow. After growth, 3D GF was cut into piece of 5 mm × 5 mm (1.5 mm thick) and then removed the nickel substrate by incubation with 3 M HCl. After etching the nickel, the obtained 3D GF was cleaned by deionized water prior to use.

2.3. Preparation of modified electrodes

The bare glassy carbon electrode (GCE) was first polished with 0.3 and 0.05 μm alumina slurries and washed with ethanol and water three times, and dried under nitrogen. Then, one piece of 3D GF (5 mm × 5 mm, 1.5 mm thick) was scooped up using glass rod from deionized water, then fixed on the GCE and dried in air at room temperature for about 24 h naturally. Then, the 3D GF modified GCE was immersed into a SDBS solution (2.87 mM) overnight to obtain 3D GF/SDBS HM nanocomposite modified GCE. For comparison, 3D GF/dodecyl trimethyl ammonium bromide (DTAB) hemimicelle nanocomposite modified GCE was also prepared using the same procedures.

2.4. Physicochemical characterization

The X-ray diffraction was carried out on a Bruker AXS D8 ADVANCE X-ray diffractometer. The morphology of the composite was examined by field-emission scanning electron microscopy (Zeiss Supra 55 VP FEG). Fourier transform infrared (FT-IR) spectra of samples were recorded in the range 400–4000 cm^{-1} using FT-IR spectroscopy (Nicolet-740). The sample was prepared in a pellet form with spectroscopic-grade KBr. Static contact angles were measured on a drop shape analysis system through the image analyzer (Datephysics OCA40).

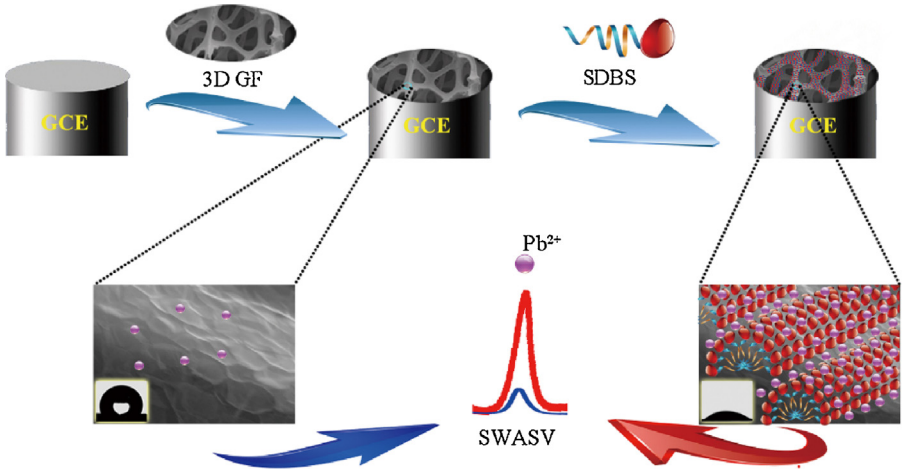

Scheme 1. Schematic representation for SWASV detection of Pb^{2+} based on the 3D GF/SDBS HM nanocomposite modified GCE.

2.5. Electrochemical measurements

All of the electrochemical experiments were performed on a VMP3 electrochemical workstation (Bio-Logic Co., Claix, France) with a conventional three-electrode cell, in which the modified GCE (d = 3 mm), Ag/AgCl (3 M KCl) electrode and platinum plate were used as working, reference, and auxiliary electrode, respectively. Cyclic voltammetric (CV) experiment were carried out with the scan rate of 50 mV s^{-1} in 5 mM $[Fe(CN)_6]^{3-}$/$[Fe(CN)_6]^{4-}$ containing 0.1 M KCl. Electrochemical impedance spectroscopy (EIS) measurement were conducted in the frequency range from 100 kHz to 0.01 Hz at open circuit potential using the same probe.

Square wave anodic stripping voltammetry (SWASV) was used for the detection of Pb^{2+} with a deposition potential of −1.2 V for 240 s in 0.1 M acetate buffer solution (pH 5.5). The anodic stripping of electrodeposited metal was performed in the potential range of −1.2 to −0.3 V with the following parameters: a pulse height of 25 mV, a pulse width of 50 ms, a step height of 4 mV. A desorption potential of 0.5 V for 50 s was performed to remove the residual metals on the electrode surface under stirring condition. After measurements, the modified electrode could be stored in air at room temperature.

3. Results and discussion

3.1. Structure characterization of 3D GF and 3D GF/SDBS HM nanocomposite

Fig. 1A, B showed the representative SEM images of 3D GF and 3D GF/SDBS HM nanocomposite, respectively. As shown in Fig. 1A, 3D GF exhibited well defined macroporous structure with the pore diameter of 100−200 μm. And the surface of graphene skeleton is smooth, assuming the identical surface topology as nickel substrate due to conformal CVD growth (the inset in Fig. 1A). XRD patterns and Raman spectrum results (Fig. S1 and S2) further indicated that 3D GF had good quality. As shown in Fig. 1B, although the macroporous structure of 3D GF/SDBS HM nanocomposite without nickel foam substrate was collapsed slightly, 3D structure remains intact. Energy-dispersive X-ray spectroscopy (EDX) confirmed that the SDBS was indeed coated on the 3D GF without any other impurities as specified in Fig. 1C. Especially, nickel impurities were not left on graphene foam as revealed by EDX (Fig. S3). Thus, 3D GF/SDBS HM nanocomposite itself contributed to the following electrocatalytic activities of the modified GCE.

The composition of 3D GF/SDBS HM nanocomposite was further examined by FTIR. In the FTIR spectra of 3D GF, there was no significant peak except the O-H stretching vibration at 3440 cm^{-1} and the peak centered at 1630 cm^{-1} contributed by the physically adsorbed water molecules from air [27,28]. Compared with that of 3D GF, several new peaks attributed to SDBS appeared in the FTIR spectrum of 3D GF/SDBS HM nanocomposite, confirming that SDBS has been adsorbed on 3D GF surfaces. The new peaks located at 2920 and 2852 cm^{-1} correspond to the asymmetrical and symmetrical stretching of $-CH_2$. The peak at 2954 cm^{-1} is attributed to the asymmetrical stretching vibration of $-CH_3$, and those at 1431 and 1358 cm^{-1} are attributed to symmetrical and asymmetrical deform vibrations of $-CH_3$. The peaks at 1589 and 1012 cm^{-1} are attributed to the C=C stretching vibration of benzenoid ring and the characteristic peak of $-SO_3^-$.

Contact angle experiments were carried out to investigate the hydrophilic/hydrophobic features of 3D GF and 3D GF/SDBS HM nanocomposite. As shown in Fig. 2, the water droplet on the surface of 3D GF/SDBS HM nanocomposite spread quickly less than 0.4 s whereas the profile of water droplet maintained in the original state for more than 2.5 s on the surface of 3D GF. The static contact angles of 3D GF and 3D GF/SDBS HM nanocomposite were

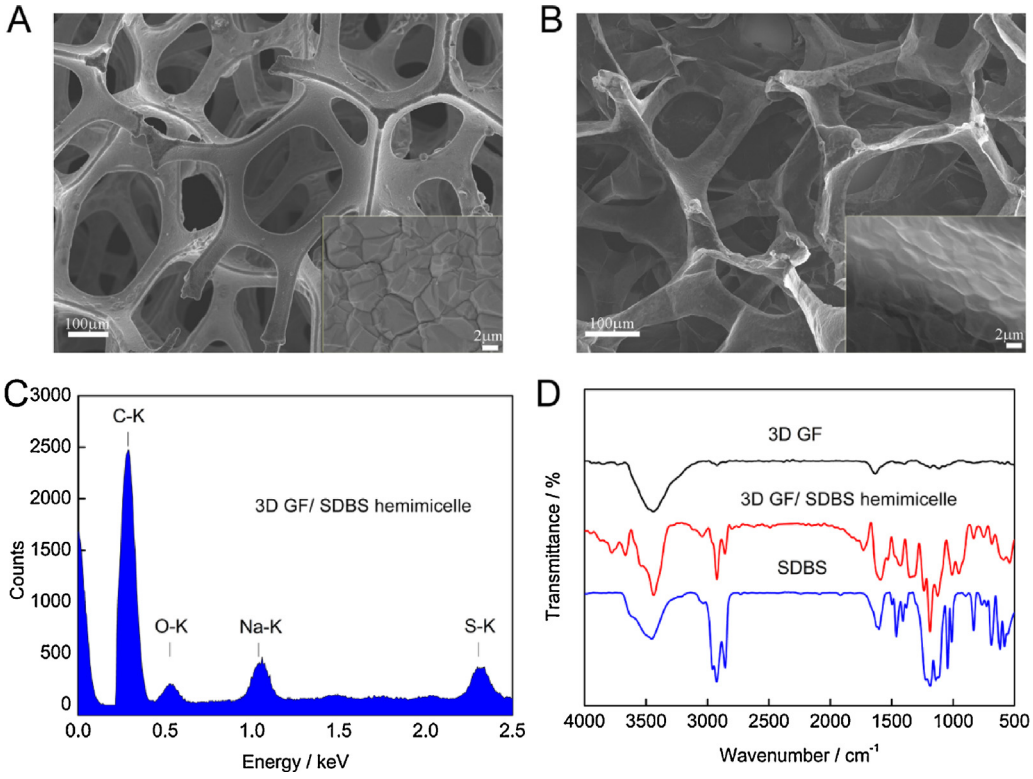

Fig. 1. SEM image of 3D GF with nickel foam substrate (A) and 3D GF/SDBS HM nanocomposite (B). The insets in A and B show the surface of 3D GF and 3D GF/SDBS HM nanocomposite at a higher magnification. (C) EDX of 3D GF/SDBS HM nanocomposite. (D) FT-IR spectra of bare 3D GF, SDBS and 3D GF/SDBS HM nanocomposite.

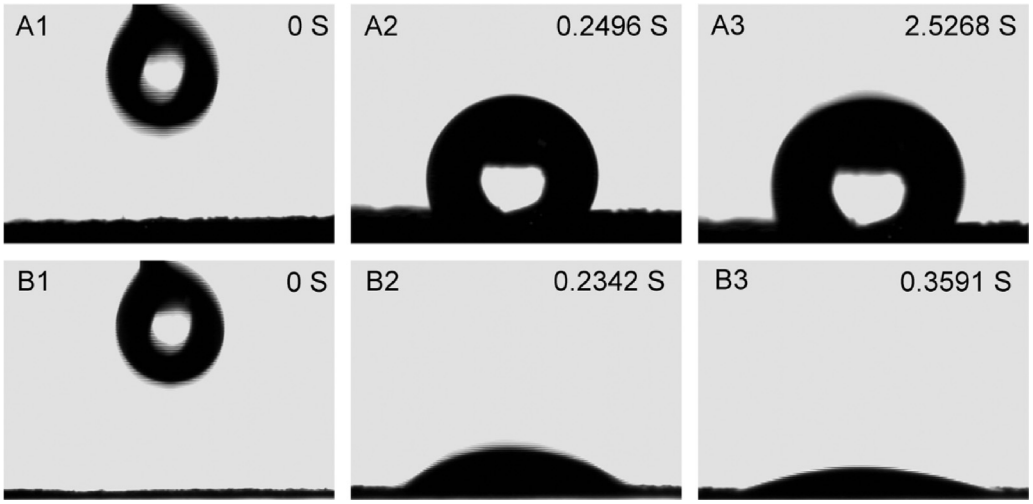

Fig. 2. Contact angle image of 3D GF (A1-3) and 3D GF/SDBS HM nanocomposite (B1-3).

measured to be 114°and 36°, respectively. Compared with 3D GF, 3D GF/SDBS HM nanocomposite showed much lower contact angle. Generally, the surfactants adsorbed on a hydrophobic surface tend to aggregate into half-cylindrical hemimicelles from both the experimental observations and computer simulations [14–16]. In these aggregates, the headgroup of the adsorbed surfactant molecules are exposed to the aqueous phase in the high-density adsorption regime. Clearly, such an orientation can explain the low contact angles of the 3D GF/SDBS hemimicelle nanocomposite. Compared with the relatively hydrophobic interface of 3D GF, 3D GF/SDBS HM nanocomposite is comparatively more hydrophilic.

3.2. Physicochemical characterization

Electrochemical impedance spectroscopy (EIS) was first employed to characterize the interface properties of the bare GCE and other modified electrodes. In a typical Nyquist plot, the electron-transfer resistance (Ret) was corresponded to the diameter of semicircle portion at higher frequency range [29]. As seen in Fig. 3A, the Ret value of the 3D GF modified GCE was smaller than that of bare GCE, on account of the high electrical conductivity of graphene and the vastly multiplexed conductive pathways provided by the 3D GF [10]. After modification with SDBS, the 3D GF/SDBS HM nanocomposite modified GCE showed a significantly larger Ret than 3D GF modified GCE, which is attributed to the repulsion between negatively charged SDBS and $[Fe(CN)_6]^{3-}$/$[Fe(CN)_6]^{4-}$ ion pair.

The performance of the bare GCE and other modified electrodes in the cyclic voltammetric mode was tested with 5 mM $[Fe(CN)_6]^{3-}$/$[Fe(CN)_6]^{4-}$ in 0.1 M KCl and the results are presented in Fig. 3B. It is noted that the electrochemical signal from the 3D GF modified GCE is 4-fold larger than that from bare GCE, indicating that the 3D GF modified GCE has a much higher charge transfer rate and large specific surface area. The decreased voltammetric responses of 3D GF/SDBS HM nanocomposite modified GCE also can be attributed to charges repulsion of SDBS and $[Fe(CN)_6]^{3-}$/$[Fe(CN)_6]^{4-}$ redox probe, which further illustrated the modification with SDBS on the surface of 3D GF.

Fig. 3C showed the SWASV analytical characteristics of different electrodes. When the adsorption process was carried out for 240 s at −1.2 V in 0.1 M acetate buffer (pH 5.5) containing 0.24 μM Pb^{2+}, one weak peak was observed at both bare (black curve) and SDBS (green curve) modified GCE in the potential range of −1.0 to −0.4 V. This indicated that SDBS modified GCE has very weak responsiveness towards Pb^{2+}, similar to bare GCE. For 3D GF (blue curve) modified GCE, there was one evident peak since 3D GF has a good conductivity and a certain absorbability toward the target lead ions due to the well-defined macroporous structure. After further modified with SDBS hemimicelles, the peak current at the 3D GF/SDBS HM nanocomposite modified GCE was remarkably enhanced. This is mainly attributed to two reasons. First, 3D GF with the high

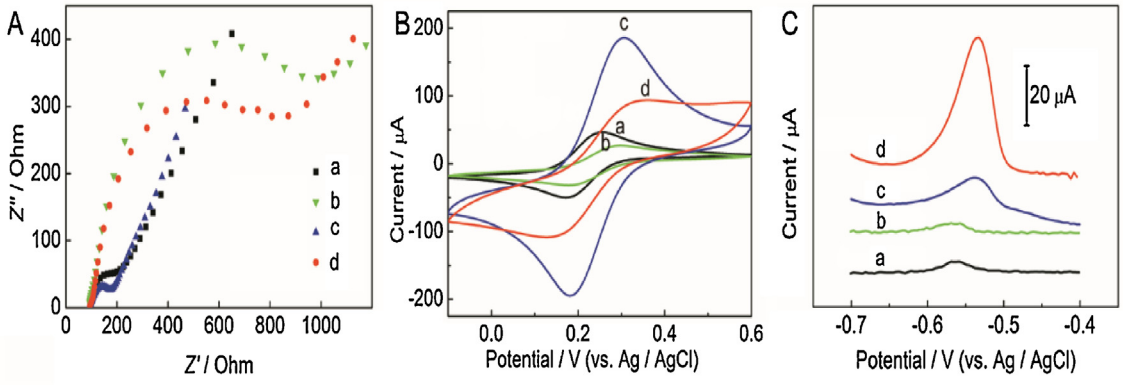

Fig. 3. Nyquist diagram of electrochemical impedance spectroscopy (A) and cyclic voltammograms (B) for bare (a), SDBS (b), 3D GF (c) and 3D GF/SDBS HM nanocomposite (d) modified GCE in the solution of 5 mM $K_3[Fe(CN)_6]$ solution containing 0.1 M KCl. (C) SWASV responds of 0.24 μM Pb^{2+} on bare (a), SDBS (b), 3D GF (c) and 3D GF/SDBS HM nanocomposite (d) modified GCE in 0.1 M acetate buffer solution (pH 5.5).

specific surface area, high conductivity and special three-dimensionally macro porous structure is in favor of charge transfer. Second, due to the high affinity between SDBS and lead ions, SDBS hemimicelles adsorbed on 3D GF surfaces can act as adsorbents to rapidly extract and concentrate lead ions from water, and hence an increased amount of lead deposited on the electrode surface.

As a control, the anionic surfactant SDBS was replaced by cationic surfactant DTAB to assess the role of electrostatic interactions in accumulation of Pb^{2+} at the surface of 3D GF/SDBS electrode. Thus, the analysis of Pb^{2+} by SWASV scanning using 3D GF/DTAB hemimicelle nanocomposite modified GCE was investigated. It was found that the peak current at the 3D GF/DTAB hemimicelle nanocomposite modified GCE was almost unchanged compared with bare GCE (Fig. S4). This further indicated that the electrostatic attraction between SDBS hemimicelles and lead ions played an important role in accumulating lead ions.

To further confirm the excellent stripping performance of 3D GF/SDBS HM nanocomposite modified GCE was attributed to SDBS hemimicelles but not SDBS monomers, the preparation of the modified electrode with different SDBS concentration was investigated. Firstly, the contact angle experiments were carried out to investigate hydrophilic/hydrophobic features of 3D GF/SDBS HM nanocomposite with different SDBS concentration. The contact angle of 3D GF/SDBS HM nanocomposite against SDBS concentration was shown in Fig. 4 (square). As shown, the contact angle decreases sharply towards a plateau region at about SDBS concentration of 2.4 mM, indicating the formation of SDBS hemimicelles on 3D GF surfaces. Fig. 4 (circle) also showed the stripping peak current for lead ions against SDBS concentration. As shown in Fig. 4, the stripping peak current for lead ions increases slowly at low SDBS concentration, and then increases sharply to a high value just over about 2.4 mM, and finally increases slowly with the further increase of SDBS concentration in the preparation of 3D GF/SDBS hemimicelles nanocomposite. At low SDBS concentration, individual SDBS molecules were adsorbed on 3D GF via the hydrophobic effect between SDBS and 3D GF. The electrostatic attraction between SDBS monomers and lead ions resulted in the accumulation of lead ions at the surface of 3D GF/SDBS HM nanocomposite modified GCE, which resulted in an increased response current with the addition of SDBS. With the increase of SDBS concentration above 2.4 mM, SDBS hemimicelles are formed on the 3D GF surface. The formed SDBS HM could concentrate trace lead ions from water and contribute to the deposition of lead ion on electrode surfaces. Notably, the accumulation and deposition efficiency of SDBS hemimicelles is much higher than that of SDBS monomers, and hence a significantly improved response current. With the further increase of SDBS concentration, the SDBS hemimicelles density on 3D graphene increased, so the accumulation and deposition efficiency of the modified GCE also improved, resulting in a continuous peak current enhancement. The results here indicated that 3D GF/SDBS hemimicelle nanocomposite could be a promising electrode material for the detection of lead ions.

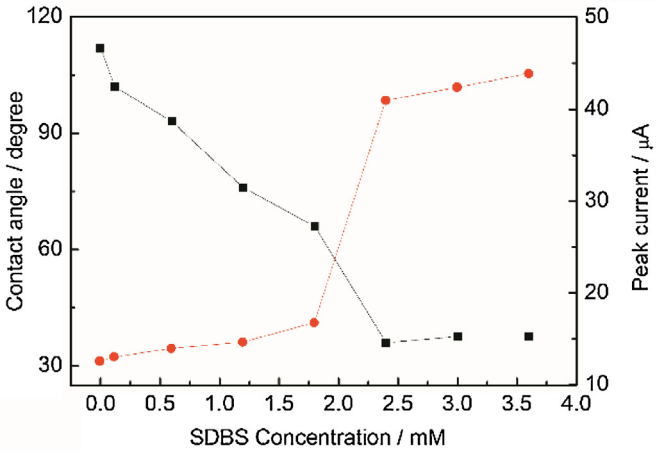

Fig. 4. Contact angle of 3D GF/SDBS HM nanocomposite (square) and SWASV response (circle) of 0.24 μM Pb^{2+} on the 3D GF/SDBS HM nanocomposite modified GCE against SDBS concentrations.

3.3. Optimization of detection conditions

In order to achieve the maximum sensitivity for Pb^{2+} detection with 3D GF/SDBS HM nanocomposite modified GCE, 0.1 M acetate buffer solution containing 0.24 μM Pb^{2+} was investigated to optimize the effects of different parameters, such as the pH of the acetate buffer solution, deposition potential and time.

Fig. S5A showed the effect of pH on the peak current of Pb^{2+} from pH 3.5 to 6.5. As shown, the peak current of Pb^{2+} increased as the pH increased from 3.5 to 5.5, and then decreased with the continuous increase of pH to 6.5. At lower pH, the sulfonic group of SDBS is not effectively deprotonated, which decreases the affinity of lead ions to 3D GF/SDBS hemimicelle nanocomposite due to the reduced electrostatic attraction. The decrease of peak current at higher pH may be due to the hydrolysis of lead ions. The best signals were appeared at pH 5.5, which was selected as the optimal pH for SWASV analysis. Fig. S5 B illustrated the effect of deposition potential on the peak current. When the deposition potential shifted from −0.8 to −1.2 V, Pb^{2+} is more easily reduced due to the enhanced kinetics [30]. Thus, the peak currents increased obviously and reached maximum at potential −1.2 V. When the deposition potential was more negative than −1.2 V, the peak currents decreased due to the generation of H_2. The deposition time was also studied from 60 to 480 s. We can conclude from Fig. S5C that the peak currents increased linearly with the deposition time. There is no obviously saturation effect, even with the deposition time being 480 s. Considering the high sensitivity and the practical measurement time, 240 s was selected as the deposition time.

3.4. Analytical performance

Under the optimal conditions, the 3D GF/SDBS HM nanocomposite modified GCE was applied for determination of Pb^{2+} using SWASV analysis. Fig. 5 showed the SWASV responses for different concentration of Pb^{2+} and the corresponding calibration plot. It can be seen that the peak currents of Pb^{2+} exhibit a good linear relationship with its concentration in the range from 0.48 nM to 0.97 μM. The calibration plot was calculated as $i/\mu A = 0.15\ c/nM + 1.13$, with the correlation coefficient of 0.9973. The limit of detection (LOD) was 1.45×10^{-11} M (S/N = 3), which was much lower than the limited value of 2.41×10^{-9} M in drinking water permitted by the World Health Organization (WHO) [31]. The analytical performance was also compared with other modified electrodes reported previously, which were summarized in Table 1. It showed that the proposed electrode exhibited a wider range, lower detection limit and higher sensitivity.

3.5. Selectivity, interference, stability and repeatability

Some other common heavy metal ions, such as Cd^{2+} and Cu^{2+}, were tested to evaluate the selectivity of 3D GF/SDBS HM nanocomposite modified GCE under the optimized conditions for Pb^{2+} detection. The obtained SWASV curves were shown in Fig. 6A. As shown, Cd^{2+} and Cu^{2+} could be detected, and the signal of Pb^{2+} is higher than that of Cd^{2+}, indicating that Pb^{2+} is

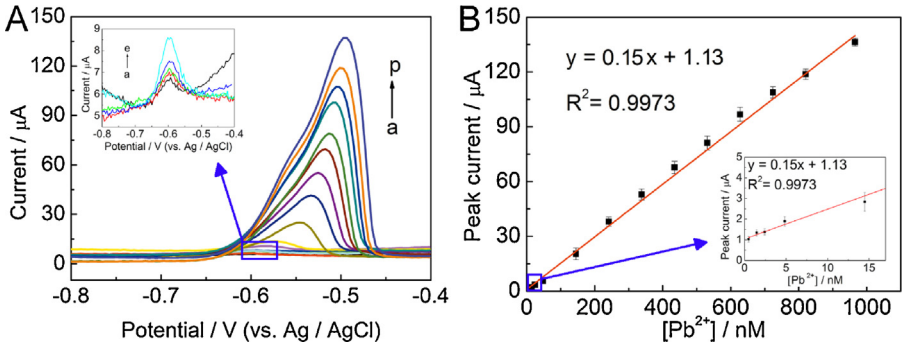

Fig. 5. (A) SWASV response of the 3D GF/SDBS HM nanocomposite modified GCE for Pb^{2+} with different concentrations (from a to p: 0.48, 1.45, 2.41, 4.83, 14.5, 24.1, 48.3, 140, 240, 340, 430, 530, 630, 720, 820, 970 nM). (B) A linear calibration plot of peak current against Pb^{2+} concentrations.

Table 1
Comparison of the electrode modified with 3D GF/SDBS HM nanocomposite and other materials for the detection of Pb^{2+} in aqueous media.

Modifier	Electrode	Technique	LOD [nM]	Linear range [nM]	[Ref]
Bi/NA/thiolated polyaniline	GCE	SWASV	0.241	0.48-145	[35]
CNF/NA	GCE	ASV	0.9	100-700	[36]
HP-β-CD-RGO/NA	GCE	SWASV	0.0942	0.1-9	[30]
Bi/Au-GN-Cys	GCE	SWASV	0.241	2.41-193	[37]
G/MWCNTs/Bi	GCE	SWASV	0.965	2.41-145	[34]
AlOOH-RGO	GCE	SWASV	0.0932	200-800	[32]
RGO/Bi nanocomposites	CPE	DPASV	2.65	96.5-579	[33]
3D GF/SDBS HM	GCE	SWASV	0.0145	0.48-970	This work

Bi: bismuth; NA: nafion; GCE: glassy carbon electrode; HP: hydroxypropyl; CD: cyclodextrin, RGO: reduced graphene oxide; CNF: carbon nanofiber; Au-GN-Cys: gold nanoparticle-graphene-cysteine composite; CPE: carbon paste electrode; MWCNTs: multi-walled carbon nanotubes.

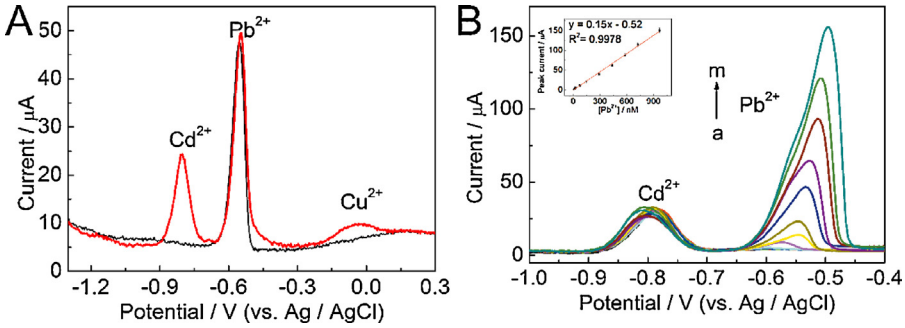

Fig. 6. (A) SWASV response of the 3D GF/SDBS HM nanocomposite modified GCE for individual analysis of 0.24 μM Pb^{2+} (black curve) and simultaneous analysis of Cd^{2+}, Pb^{2+}, Cu^{2+} at 0.24 μM (red curve) in 0.1 M acetate buffer solution (pH 5.5). (B) SWASV response of the 3D GF/SDBS HM nanocomposite modified GCE for Pb^{2+} with different concentrations (from a to m: 0.48, 1.45, 2.41, 4.83, 14.5, 24.1, 70, 140, 290, 430, 580, 720, 970 nM) in the presence of 0.44 μM Cd^{2+} in 0.1 M acetate buffer solution (pH 5.5).

competitively adsorbed by 3D GF/SDBS HM nanocomposite modified GCE. Since Cd^{2+} was stripped with the appearance of stripping peak at different position, the presence of 0.44 μM Cd^{2+} would not interfere the determination of pb^{2+}. Furthermore, the mutual interference was further studied to demonstrate the effect of Cd^{2+} on the detection of Pb^{2+}. On fixing the concentration of Cd^{2+} and increasing the concentration of Pb^{2+} (Fig. 6B), the peak current of Pb^{2+} increased linearly while that of Cd^{2+} almost remained the same. The peak current of Pb^{2+} increased proportionally to the concentration range from 0.48 nM to 0.97 μM. The linear equation was $i/\mu A = 0.15\ c/nM - 0.52$, with correlation coefficient of 0.9978. The detection slope of Pb^{2+} was the same to that shown in Fig. 5 (0.15 versus 0.15), which indicates that there is no mutual interference between Pb^{2+} and Cd^{2+}. As shown in the above section, the electrostatic attraction between SDBS and heavy metal ions played important roles in accumulating heavy metal ions. Therefore, the selectivity towards Pb^{2+} may be attributed to the effective formation of ion-pair complexes of surfactant with the Pb^{2+} [24]. The selective behavior of 3D GF/SDBS HM nanocomposite modified GCE with regard to Pb^{2+} can also be explained by the turbidity results (Fig. S6). Although the addition of Cu^{2+}, Cd^{2+} and Zn^{2+} exhibited a limited turbidity increases, the added Pb^{2+} resulted in an apparently increased turbidity, indicating the selectively enhanced interaction between Pb^{2+} and SDBS.

The interference study was also performed by adding various ions into acetate buffer solutions containing 0.24 μM Pb^{2+}. Under ± 5% relative error, it was found that 500-fold Na^{+}, K^{+}, Cl^{-}, NO_3^{-}, SO_4^{2-}, PO_4^{3-}, 100-fold Al^{3+}, Mg^{2+}, 10-fold Zn^{2+}, and 3-fold Ni^{2+}, had no significant effect on the peak current of Pb^{2+}. Notably, the added Cu^{2+} could reduce the SWASV respond of lead ion due to the formation of intermetallic compounds [32,38]. Although the added Cu^{2+} with the same concentration has no

influence on the respond of Pb^{2+} (Fig. 6A), the peak current of Pb^{2+} decreased more than 20% when 5-fold Cu^{2+} was added. This indicated Cu^{2+} with high concentration also could bind to the 3D GF/SDBS HM nanocomposite modified GCE surface to some extent. Thus, 0.1 mM ferricyanide was selected to exclude the interference of Cu^{2+}. Note that Tl^{+} is generally considered as interference in the determination of Pb^{2+} in ASV measurements because of the proximity of their peaks. Unfortunately, Tl^{+} cannot be obtained in our laboratory due to its high toxicity. Alternatively, the effect of In^{3+} on the peak current of Pb^{2+} was studied since Tl^{+} and In^{3+} have very close stripping potentials. Under ± 5% relative error, 3-fold In^{3+} had no significant effect on the peak current of Pb^{2+}. We also studied the influence of 96-fold Triton X-100 and 276-fold humic acids on the detection of Pb^{2+}. Under ± 5% relative error, both Triton X-100 and humic acids had no significant effect on the peak current of Pb^{2+}.

The stability of the 3D GF/SDBS HM nanocomposite modified GCE was investigated by 15 time repetitive measurements of SWASV response for 0.24 μM Pb^{2+}. As shown in Fig. 7, the stripping current of the electrode is highly reproducible with a relative standard deviation (RSD) of 2.1%. Furthermore, the response sensitivity retained a value of more than 97% over two months. Therefore, the 3D GF/SDBS HM nanocomposite modified GCE has an excellent stability for repetitive stripping measurements. The reproducibility of different electrodes was estimated by comparing the stripping peak current of 0.24 μM Pb^{2+} at different electrodes (n = 5). Here, the RSD value was 4.78%, revealing the good repeatability between different electrodes.

3.6. Real sample analysis

The feasibility of the detection method using 3D GF/SDBS HM nanocomposite modified GCE was investigated by detecting Pb^{2+} in natural water samples (from Slender West Lake in Yangzhou, P. R. China). The water samples were filtered through a 0.8 μm membrane prior to detection. There was 8.93 nM Pb^{2+} obtained by the present SWASV analysis in the water sample, which is very similar to the lead ion concentration (8.88 nM) obtained by inductively coupled plasma mass spectrometry (ICP-MS) method. The recovery studies were carried out on real samples to further investigate the feasibility of 3D GF/SDBS HM nanocomposite modified GCE. As shown in Table 2, the recovery obtained is 97.9–102.9%, revealing that the 3D GF/SDBS HM nanocomposite modified GCE could be used for the accurate detection of trace heavy metals in real samples and has important practical application potential.

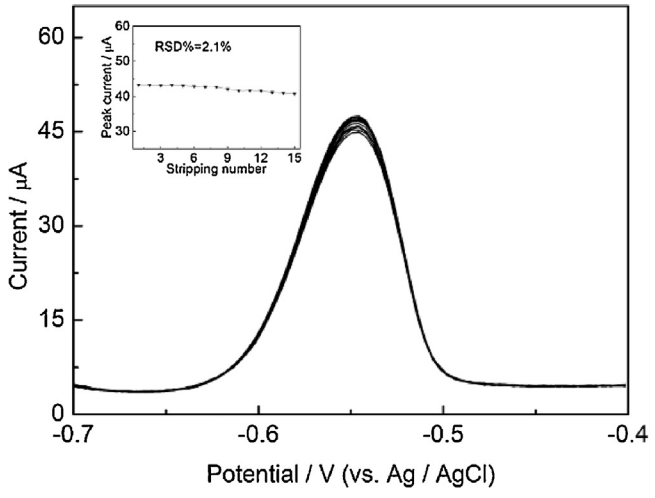

Fig. 7. The stability of SWASV response for 0.24 μM Pb^{2+} on the 3D GF/SDBS HM nanocomposite modified GCE in 0.1 M acetate buffer solution (pH 5.5).

Table 2
Determination of Pb^{2+} in lake water sample with the 3D GF/SDBS HM nanocomposite modified GCE (n = 5).

Added [nM]	Found [nM]	Recovery [%]	RSD [%]
–	8.93	–	3.9
9.65	18.38	97.9	2.3
19.30	28.72	102.5	2.8
28.95	38.71	102.9	3.3

4. Conclusion

In this work, we demonstrated a novel electrochemical sensor based on three-dimensional graphene/sodium dodecyl benzene sulfonate hemimicelle nanocomposites. The nanocomposite was characterized by SEM, FTIR, XRD and contact angle experiments. Through a combination of hemimicelle's excellent accumulating ability, and the outstanding electronic and specific area properties of 3D graphene, this electrode material showed high sensitivity for electrochemical detection of Pb^{2+} by square wave anodic stripping voltammetry. Under the optimum conditions, as low as 0.145 nM Pb^{2+} can be detected with a broad linear range from 0.48 nM to 0.97 μ M Pb^{2+}. The sensor was further applied to the determination of lead ion in real water sample with good results. It is expected that this simple, ultrasensitive, and stable electrochemical sensor shows considerable potential applications in environmental, biological and food analysis.

Acknowledgments

This work was supported by the National Nature Science Foundations of China (21173182, 21573190), PAPD and Nature Science Key Basic Research of Jiangsu Province for Higher Education (15KJA150009).

Appendix A. Supplementary data

Supplementary data associated with this article can be found, in the online version, at http://dx.doi.org/10.1016/j.electacta.2016.06.136.

References

[1] L. Järup, Hazards of heavy metal contamination, British medical bulletin 68 (2003) 167–182.
[2] G. Aragay, J. Pons, A. Merkoci, Recent Trends in Macro-, Micro-, and Nanomaterial-Based Tools and Strategies for Heavy-Metal Detection, Chem. Rev, 1 11 (2011) 3433–3458.
[3] J. Gong, T. Zhou, D. Song, L. Zhang, X. Hu, Stripping voltammetric detection of mercury (II) based on a bimetallic Au- Pt inorganic- organic hybrid nanocomposite modified glassy carbon electrode, Anal. Chem. 82 (2009) 567–573.
[4] L. Cui, J. Wu, H. Ju, Electrochemical sensing of heavy metal ions with inorganic, organic and bio-materials, Biosens. Bioelectron. 63 (2015) 276–286.
[5] G. Aragay, A. Merkoci, Nanomaterials application in electrochemical detection of heavy metals, Electrochim. Acta 84 (2012) 49–61.
[6] Y. Shao, J. Wang, H. Wu, J. Liu, I.A. Aksay, Y. Lin, Graphene Based Electrochemical Sensors and Biosensors: A Review, Electroanalysis 22 (2010) 1027–1036.
[7] Z. Chen, W. Ren, L. Gao, B. Liu, S. Pei, H.M. Cheng, Three-dimensional flexible and conductive interconnected graphene networks grown by chemical vapour deposition, Nat Mater 10 (2011) 424–428.
[8] X. Cao, Y. Shi, W. Shi, G. Lu, X. Huang, Q. Yan, Q. Zhang, H. Zhang, Preparation of novel 3D graphene networks for supercapacitor applications, Small 7 (2011) 3163–3168.
[9] T. Maiyalagan, X. Dong, P. Chen, X. Wang, Electrodeposited Pt on three-dimensional interconnected graphene as a free-standing electrode for fuel cell application, J. Mater. Chem. 22 (2012) 5286–5290.

[10] X.C. Dong, X.W. Wang, L.H. Wang, H. Song, H. Zhang, W. Huang, P. Chen, 3D Graphene Foam as a Monolithic and Macroporous Carbon Electrode for Electrochemical Sensing, ACS Appl. Mater. Interfaces 4 (2012) 3129–3133.
[11] J.Y. Liu, J. Wang, T.S. Wang, D. Li, F.N. Xi, J. Wang, E.K. Wang, Three-dimensional electrochemical immunosensor for sensitive detection of carcinoembryonic antigen based on monolithic and macroporous graphene foam, Biosens. Bioelectron. 65 (2015) 281–286.
[12] X.C. Dong, Y.F. Cao, J. Wang, M.B. Chan-Park, L.H. Wang, W. Huang, P. Chen, Hybrid structure of zinc oxide nanorods and three dimensional graphene foam for supercapacitor and electrochemical sensor applications, RSC Adv. 2 (2012) 4364–4369.
[13] R. Sitko, P. Janik, B. Feist, E. Talik, A. Gagor, Suspended Aminosilanized Graphene Oxide Nanosheets for Selective Preconcentration of Lead Ions and Ultrasensitive Determination by Electrothermal Atomic Absorption Spectrometry, ACS Appl. Mater. Interfaces 6 (2014) 20144–20153.
[14] S. Bandyopadhyay, J.C. Shelley, M. Tarek, P.B. Moore, M.L. Klein, Surfactant aggregation at a hydrophobic surface, J. Phys. Chem. B 102 (1998) 6318–6322.
[15] E.J. Wanless, W.A. Ducker, Organization of sodium dodecyl sulfate at the graphite-solution interface, J. Phys. Chem. 100 (1996) 3207–3214.
[16] Z. Kiraly, G. Findenegg, Calorimetric evidence of the formation of half-cylindrical aggregates of a cationic surfactant at the graphite/water interface, J. Phys. Chem. B 102 (1998) 1203–1211.
[17] X. Zhao, Y. Shi, T. Wang, Y. Cai, G. Jiang, Preparation of silica-magnetite nanoparticle mixed hemimicelle sorbents for extraction of several typical phenolic compounds from environmental water samples, J. Chromatogr. A 1188 (2008) 140–147.
[18] W. Wang, B. Chen, Y. Huang, Eggshell membrane-based biotemplating of mixed hemimicelle/admicelle as a solid-phase extraction adsorbent for carcinogenic polycyclic aromatic hydrocarbons, J. Agric. Food Chem. 62 (2014) 8051–8059.
[19] F. Merino, S. Rubio, D. Pérez-Bendito, Solid-phase extraction of amphiphiles based on mixed hemimicelle/admicelle formation: Application to the concentration of benzalkonium surfactants in sewage and river water, Anal. Chem. 75 (2003) 6799–6806.
[20] A. Ballesteros-Go'mez, S. Rubio, Hemimicelles of alkyl carboxylates chemisorbed onto magnetic nanoparticles: study and application to the extraction of carcinogenic polycyclic aromatic hydrocarbons in environmental water samples, Anal. Chem. 81 (2009) 9012–9020.
[21] D. Xiao, D. Yuan, H. He, C. Pham-Huy, H. Dai, C. Wang, C. Zhang, Mixed hemimicelle solid-phase extraction based on magnetic carbon nanotubes and ionic liquids for the determination of flavonoids, Carbon 72 (2014) 274–286.
[22] L. Li, Y. Huang, Y. Wang, W. Wang, Hemimicelle capped functionalized carbon nanotubes-based nanosized solid-phase extraction of arsenic from environmental water samples, Anal. Chim. Acta 631 (2009) 182–188.
[23] C. Li, L. Chen, W. Li, Magnetic titanium oxide nanoparticles for hemimicelle extraction and HPLC determination of organophosphorus pesticides in environmental water, Microchim. Acta 180 (2013) 1109–1116.
[24] N. Iqbal, M.Z.A. Rafiquee, Synthesis and characterization of lead(II) selective sodium dodecyl benzene sulphonate–cerium(IV) phosphate ion exchanger, Colloids and Surfaces A: Physicochemical and Engineering Aspects 364 (2010) 67–71.
[25] R.F. Pereira, A.J. Valente, H.D. Burrows, The interaction of long chain sodium carboxylates and sodium dodecylsulfate with lead(II) ions in aqueous solutions, J Colloid Interface Sci 414 (2014) 66–72.
[26] C.K. Ahn, D. Park, S.H. Woo, J.M. Park, Removal of cationic heavy metal from aqueous solution by activated carbon impregnated with anionic surfactants, J. Hazard. Mater. 164 (2009) 1130–1136.
[27] Y. Xu, H. Bai, G. Lu, C. Li, G. Shi, Flexible graphene films via the filtration of water-soluble noncovalent functionalized graphene sheets, J. Am. Chem. Soc. 130 (2008) 5856–5857.
[28] X. Dong, J. Wang, J. Wang, M.B. Chan-Park, X. Li, L. Wang, W. Huang, P. Chen, Supercapacitor electrode based on three-dimensional graphene–polyaniline hybrid, Mater. Chem. Phys. 134 (2012) 576–580.
[29] A.J. Bard, L.R. Faulkner, Electrochemical methods: fundamentals and applications, 2nd ed., John Wiley & Sons, New York, 2001.
[30] M. Lv, X. Wang, J. Li, X. Yang, C.a. Zhang, J. Yang, H. Hu, Cyclodextrin-reduced graphene oxide hybrid nanosheets for the simultaneous determination of lead (II) and cadmium(II) using square wave anodic stripping voltammetry, Electrochim. Acta 108 (2013) 412–420.
[31] F. Edition, Guidelines for Drinking-water Quality, WHO chronicle 38 (2011) 104–108.
[32] C. Gao, X.Y. Yu, R.X. Xu, J.H. Liu, X.J. Huang, AlOOH-Reduced Graphene Oxide Nanocomposites: One-Pot Hydrothermal Synthesis and Their Enhanced Electrochemical Activity for Heavy Metal Ions, ACS Appl. Mater. Interfaces 4 (2012) 4672–4682.
[33] P.K. Sahoo, B. Panigrahy, S. Sahoo, A.K. Satpati, D. Li, D. Bahadur, In situ synthesis and properties of reduced graphene oxide/Bi nanocomposites: As an electroactive material for analysis of heavy metals, Biosens. Bioelectron. 43 (2013) 293–296.
[34] H. Huang, T. Chen, X.Y. Liu, H.Y. Ma, Ultrasensitive and simultaneous detection of heavy metal ions based on three-dimensional graphene-carbon nanotubes hybrid electrode materials, Anal. Chim. Acta 852 (2014) 45–54.
[35] L. Chen, Z. Su, X. He, Y. Liu, C. Qin, Y. Zhou, Z. Li, L. Wang, Q. Xie, S. Yao, Square wave anodic stripping voltammetric determination of Cd and Pb ions at a Bi/Nafion/thiolated polyaniline/glassy carbon electrode, Electrochem. Commun. 15 (2012) 34–37.
[36] D.L. Zhao, T.T. Wang, D. Han, C. Rusinek, A.J. Steckl, W.R. Heineman, Electrospun Carbon Nanofiber Modified Electrodes for Stripping Voltammetry, Anal. Chem. 87 (2015) 9315–9321.
[37] L. Zhu, L.L. Xu, B.Z. Huang, N.M. Jia, L. Tan, S.Z. Yao, Simultaneous determination of Cd(II) and Pb(II) using square wave anodic stripping voltammetry at a gold nanoparticle-graphene-cysteine composite modified bismuth film electrode, Electrochim. Acta 115 (2014) 471–477.
[38] R.J. Grim, Catalytic Activity of an Intermetallic Compound of Cadmium and Copper in the Vapor-phase Reduction of Nitrobenzene, J. Phys. Chem. 46 (1942).